ACS APPLIED ENERGY MATERIALS

www.acsaem.org

Article

Investigating Surface Reactivity of a Ni-Rich Cathode Material toward CO_2, H_2O, and O_2 Using Ambient Pressure X-ray Photoelectron Spectroscopy

Heyin Chen,* Tove Ericson, Robert H. Temperton, Ida Källquist, Haidong Liu, Calley N. Eads, Anastasiia Mikheenkova, Margit Andersson, Esko Kokkonen, William R. Brant, and Maria Hahlin*

Cite This: *ACS Appl. Energy Mater.* 2023, 6, 11458−11467

Read Online

ACCESS | Metrics & More | Article Recommendations | Supporting Information

ABSTRACT: Layered Ni-rich transition metal oxide materials are considered the most promising cathodes for use in commercial Li-ion batteries. Due to their instability in air, an impurity layer forms during storage under ambient conditions, and this layer increases electrochemical polarization during charging and discharging, which ultimately leads to a lower cycling capacity. In this work, we found that storage of the $LiNi_{0.8}Mn_{0.1}Co_{0.1}O_2$ (NMC 811) material in ultrahigh vacuum (UHV) can restore the surface by reducing the amount of native carbonate species in the impurity layer. In this work, in situ soft X-ray ambient pressure photoelectron spectroscopy is used to directly follow the interaction between common gases found in air and the NMC 811 surface. During gas exposure of the NMC 811 surface to pure CO_2, O_2, and a mixture of both pure gases, surface-adsorbed CO_2 or/and O_2 were detected; however, permanent changes could not be identified under UHV after the gas exposure. In contrast, a permanent increase in metal hydroxide species was observed on the sample surface following H_2O vapor exposure, and an increased intensity in the carboxylate peak was observed after exposure to a mixture of $CO_2/O_2/H_2O$. Thus, the irreversible degradation reaction with CO_2 is triggered in the presence of H_2O (on relevant time scales defined by the experiment). Additional measurements revealed that X-ray irradiation induces the formation of metal carbonate species on the NMC 811 surface under CO_2 and H_2O vapor pressure.

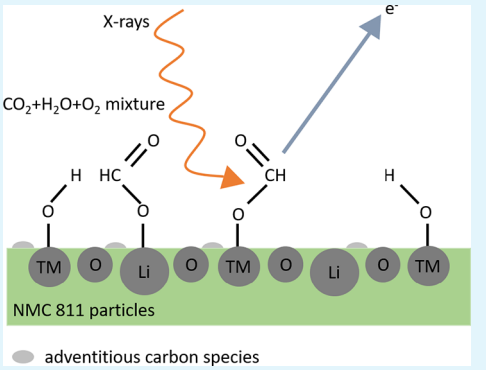

KEYWORDS: *Ni-rich NMC materials, Li-ion batteries, gas exposure, ambient pressure PES, beam effect, surface degradation*

INTRODUCTION

In recent decades, lithium-ion batteries (LIBs) have been heavily utilized in mobile phones, electric vehicles, and other portable electrical devices. According to the forecasts, by 2035, more than half of the contribution to new vehicle sales will originate from electric cars.[1] This electrification of the transport sector is an important step to reduce the global consumption of fossil fuels, but it will require further development of LIBs in terms of, for example, cost, safety, energy density, charge/discharge capacity, and so on. Recently, a lithium nickel manganese cobalt oxide ($LiNi_xMn_yCo_zO_2$, referred to as NMC) cathode material has gained huge attention in electrical vehicle applications due to its lower cost and less toxic content of Co compared to that of lithium cobalt oxide (LCO). The initial discharge capacity has been reported as 163 mAh g^{-1} for NMC 111, 175 mAh g^{-1} for NMC 532, and 203 mAh g^{-1} for NMC 811 electrodes when cycled between 3.0 and 4.3 V at 0.1 C.[2] This is linked to a higher relative concentration of Ni compared to those of Co and Mn, which enables the extraction of extra Li ions from NMC materials. This makes Ni-rich NMC materials obtain higher specific capacities becoming the most promising candidate for the next-generation cathode materials in LIBs.[3,4]

A drawback with the NMC materials is that at high states of charge, Ni-rich NMC electrodes experience increased impedance, which is assumed to originate from oxygen release from the NMC bulk structure.[5,6] The released oxygen reacts with ethylene carbonate (commonly used as a cosolvent in LIBs), leading to electrolyte degradation and CO_2 and CO generation. The reactivity of surface oxygen (terminal oxygen) is higher for Ni−O bonds than for both Mn−O and Co−O bonds in layered NMC materials,[3,7] overall resulting in a higher interfacial reactivity of NMC 811 than lower Ni-content NMCs. During battery cycling, Ni-rich NMC particles are thus more prone to react with the electrolyte, leading to faster aging

Received: June 30, 2023
Revised: October 22, 2023
Accepted: October 23, 2023
Published: November 3, 2023

in NMC 811 than in NMC 111 during electrochemical cycling.[2,7] In addition, it has also been reported that the Ni-rich NMC surface is sensitive to air, and storage under ambient conditions can lead to the formation of a degradation layer (or impurity layer) on the NMC particles.[4,7−10] For example, NMC 811 stored in air for 1 year shows significantly higher impedance growth and worse capacity retention during cycling compared to electrodes stored for 3 months.[7] The decrease in the battery cycling performance is ascribed to the formation of the degradation layer. Some researchers claim that LiOH will form on the surface of Ni-rich NMC due to water vapor exposure, and if CO_2 gas is subsequently introduced, Li_2CO_3 will be generated on the basis of LiOH formation.[11] The chemical species present in the degradation layer are still not fully determined, and the reaction mechanisms leading to these products during exposure to $CO_2/H_2O/O_2$ have not been investigated with in situ measurements. Investigating the surface chemistry and its reactivity is a crucial step, not only for understanding the mechanism of the degradation layer formation[12] but also for gaining insights into the subsequent development of water-based Ni-rich electrode processing.[13]

In this work, we show how ultrahigh vacuum (UHV) storage can be used to remove the native carbonate species from the pristine NMC 811 surface. Furthermore, the interactions between NMC 811 and single gases CO_2, H_2O, and O_2, as well as gas mixtures of CO_2/O_2 and $CO_2/H_2O/O_2$ were followed by using ambient pressure photoelectron spectroscopy (APPES) to determine the surface reactions. The two gas mixtures mimic dry room and ambient conditions, respectively. The changes in the composition of the outermost layer (around 2 nm) on the sample surface are followed in situ, and the results are compared to those measured under UHV before and after gas exposure. The results show that no permanent changes occur on the NMC 811 surface after exposure to a single gas (CO_2 or O_2) and the CO_2/O_2 mixture. However, following exposure to pure H_2O and a mixture of $CO_2/H_2O/O_2$, metal hydroxide and carboxylate are generated on the surface, respectively. Within the time frame of the experiment, these species also remained on the NMC 811 surface once the sample was placed back under UHV. Finally, we present data on how X-ray irradiation introduces composition changes on the NMC 811 surface under UHV and gas pressure conditions. It was found that the effect of X-ray exposure is less significant under UHV but still observable during 1 h measurements, e.g., O−C═O species decomposed after 70 min of exposure to X-rays. We also discovered that under CO_2 or H_2O gas pressure, carbonate species were generated during X-ray irradiation. This finding reveals that X-ray-induced effects should be acknowledged and minimized when studying air-sensitive materials with APPES for battery research and other metal catalyst research.

EXPERIMENTAL SECTION

Material Preparation. The single-crystal NMC 811 material employed in this study was tailor-made by Heliume Tech (China). The XRD pattern and SEM image of the material can be found in Figure S1 (Supporting Information). The synthesized NMC 811 was stored for around 10 days inside an Ar-filled glovebox (SIEMENS, Germany. O_2 < 1 ppm and H_2O < 1 ppm) before performing APPES measurements. NMC 811 pellets were prepared by pressing NMC 811 powder for 20 s using a 1 ton by 8 mm Die Set (MAASSEN GmbH, Germany) using the hydraulic press inside an Ar-filled glovebox. The thickness of the resulting pellets was roughly 0.5 mm. The pellets were attached to stainless steel omicron sample plates using conductive adhesive PELCO tabs (Ted Pella, Inc. Eight mm). All the samples were delivered to the MAX IV Laboratory in an airtight aluminum pouch pumped to 25 mbar using a vacuum sealer. Samples were stored under UHV for about 3 days prior to measurement which, as shown later, helps remove carbonates from the samples under UHV.

CO_2 gas (Linde) with a purity of 99.9993% (with N_2 < 5 ppm, O_2 < 2 ppm, H_2O < 2 ppm, C_nH_m < 2 ppm, and CO < 1 ppm) and O_2 gas (Linde) with a purity of 99.999% were used without any further purification. Deionized water (Milli-Q) was purified via three cycles of freeze−pump−thaw before introduction to the ambient pressure cell during the measurements.

Methods. APPES measurements were performed at the SPECIES beamline at the MAX IV laboratory, Lund, Sweden, using the APXPS endstation.[14] The identical samples (pellets) were measured under UHV before gas exposure and upon gas exposure of CO_2, H_2O, and O_2 and a mixture of CO_2/O_2 and $CO_2/H_2O/O_2$. For each gas, one sample was measured; however, repeated spectra on several different spots were measured, showing consistent results. Based on the low H_2O pumping efficiency of the instrument and considering the fact that the samples are sensitive to X-rays, we decided to use a rather low gas pressure for these measurements. Exact experimental parameters dealing with gas pressure and gas exposure time are given in Table 1.

Table 1. Five Sets of In Situ APPES Measurements with the Corresponding Gas(es), Gas Pressures, and Gas Exposure Times on NMC 811

gas condition	gas pressure (mbar)	gas exposure time (min)
CO_2	1.2×10^{-3}	40
H_2O	7×10^{-3}	30
O_2	2.4×10^{-3}	20
$CO_2 + O_2$	3.4×10^{-2}	50
$CO_2 + H_2O + O_2$	2.5×10^{-2}	55

For measurements, the spectrometer slit was set to 1 mm, and a pass energy of 50 eV was used. The angle between the electron analyzer and the synchrotron beam was set to 57.5 degree. The beam slit was set with 100 um for ambient pressure conditions and kept the same during UHV measurements to maintain the same energy resolution. During gas introduction, the core-level spectra of C 1s and O 1s were recorded as a function of gas pressure and gas exposure time. Full sets of core-level PES measurements were obtained before, during, and after gas exposure. However, due to X-ray-induced effects, data was always acquired on a fresh spot with very limited X-ray exposure time, and no sign of beam effect could be seen within the time frame of the measured and presented spectra, except in the section focused on the X-ray irradiation effect. C 1s and O 1s spectra were obtained with a photon energy of 435 and 680 eV, respectively, which gives comparable depth profiling with similar kinetic energy of the photoelectrons (~150 eV). Li 1s spectra were collected with a photon energy of 435 eV. Ni 2p (Figure S2), Co 2p (Figure S3a), Mn 2p (Figure S3b), and survey spectra (Figure S4) (Supporting Information) were measured with a photon energy of 1020 eV. No contaminations can be seen except for adventitious carbon species. C 1s measurements were recorded at every photon energy and utilized for energy calibration.

In the section addressing X-ray irradiation-induced effects, both C 1s and O 1s spectra were carried out with a photon energy of 680 eV and a beam exit slit of 100 um. These settings yield an approximate X-ray flux of 1.7×10^{11} photons/s with an irradiation spot size of approximately 60 × 120 um.

The curve fitting of the spectra was performed with Igor Pro 9 package software combining Lorentzian and Gaussian functions. The full width at half-maximum is held fixed to 0.2 eV for the Lorentzian function and is allowed to vary between 1 and 1.3 eV for the Gaussian function. A linear background was used for C 1s, O 1s and Li 1s, and each assigned peak position is fixed with a deviation of 0.1 eV. More details of the fitting parameters of C 1s, O 1s, and Li 1s have been

https://doi.org/10.1021/acsaem.3c01621
ACS Appl. Energy Mater. 2023, 6, 11458−11467

Table 2. XPS peak fitting parameters for elements (C 1s, O 1s, and Li 1s) in NMC 811

	peak assignment	binding energy (eV)		peak assignment	binding energy (eV)		peak assignment	binding energy (eV)
C 1s	C−H/C−H	285	O 1s	M-O	~528.8	Li 1s	Li lattice	~53.8
	C−O	~286.5		M−OH	~530.4		$LiOH/Li_2CO_3$	54.5−54.9
	O═C−O	~288.5		CO_3^{2-}	~531.3		surface Li (unassigned)	~55.8
	CO_3^{2-}	~289.5		O−C═O	~532.3			
				C−O	~533.5			

listed in Table 2.[15−18] Energy calibrations were referenced to the adventitious carbon peak at 285.0 eV binding energy,[7,1920] if not otherwise stated in the text. Even though adventitious carbon at 285 eV may not always be considered as a reliable "absolute" value, in this case it can act as a reliable internal reference allowing comparison between the samples.

RESULTS AND DISCUSSION

In the following, we first present the impact of UHV storage for 3 days. This is followed by the in situ NMC 811 APPES results arranged based on the introduced gases; single gas exposure to CO_2, H_2O, and O_2; and then mixed gas exposure of CO_2/O_2 and $CO_2/H_2O/O_2$, respectively. In order to follow the surface reactions, the samples are studied under UHV before and after exposure to the different gases. Finally, the impact of X-ray irradiation for ~15−20 min under ambient pressure on NMC 811 surface composition are investigated.

We highlight that due to significant X-ray irradiation effects on NMC 811 surface composition under ambient pressure, the presented spectra collected under all gas exposures were obtained on a fresh/non-X-ray exposed spot. For the in situ measurements finished under UHV conditions, the C 1s, O 1s, and Li 1s spectra were collected on the same spot within 10 min to minimize the X-ray irradiation-induced effects. The extent of modifications due to extended X-ray exposure is discussed further in the final section.

Changes in Surface Composition during Storage under UHV. In order to study the surface reactivity of NMC 811 with various gases, any initial surface impurities should ideally be removed. However, for these mesoporous NMC 811 materials, it is hard to obtain an ideally cleaned surface without any adventitious carbon species while at the same time not creating a highly reactive surface when using Ar-sputtering. In this work, we have instead used storage under UHV as a means for cleaning/refreshing the sample surface. Upon storage under UHV for up to ~80 h, the NMC 811 surface undergoes substantial changes. As shown in the C 1s spectrum in Figure 1, carbonate species reside on the as-prepared NMC 811 surface, and this clearly decreased in intensity after the sample is stored under UHV for around 16 h. After storage for 3 days under UHV, the carbonate assigned peak lost most of its intensity in the C 1s spectra compared to the as-prepared NMC 811 spectrum. However, the intensity of the O−C═O and C−H peaks increased somewhat after 3 days of UHV treatment. The increase could be linked to the surface sensitivity of PES where the removal of a top layer of carbonates may expose O−C═O and C−H, thus resulting in an intensity enhancement. A different method for removing the native surface layer was evaluated, and storage under UHV proved to be best; see Figure S5 (Supporting Information). For all in situ measurements presented below, the refreshed NMC 811, i.e., samples stored under UHV conditions for 3 days, were used. An example of the surface homogeneity has been given in Figure S6 (Supporting Information); C 1s spectra were collected from three different spots of the UHV-

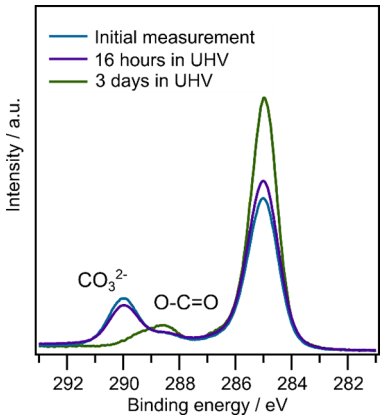

Figure 1. C 1s ($h\nu$ = 435 eV) spectra of NMC 811 after storage for various times. The spectra were binding energy calibrated by referring to the highest peak point as 285 eV, and the intensities normalized to background intensity at 281 eV.

treated sample, and no obvious changes can be noticed, except for slight variation in the C 1s hydrocarbon peak intensity. The presence of adventitious carbon species on the NMC 811 surface does not protect the NMC surface from surface impurity formation/degradation as this condition is prevalent in the case for the real material during manufacturing. In the NMC811 material that is prepared or stored under ambient conditions, CO_2 and H_2O gases can diffuse/penetrate through the interspace between particles and react with NMC 811, making NMC 811 degrade. Thus, the NMC 811 samples stored for 3 days under UHV were utilized in this experiment to obtain a surface resembling the fresh NMC811 surface.

Single Gas Exposure. *CO_2 Exposure.* Figure 2a shows C 1s spectra measured on a fresh spot under UHV before gas exposure, during CO_2 exposure at 1.2×10^{-3} mbar after the sample being exposed for around 40 min, and post CO_2, followed by O 1s and Li 1s under UHV before and after gas exposure. The UHV C 1s spectrum is fitted with peaks assigned to adventitious hydrocarbon (285.0 eV), C−O (~286.5 eV), O−C═O (~288.5 eV), and carbonate species (~ 289.5 eV) in order from low to high binding energy.[17,21,22] In O 1s, the lowest binding energy peak is assigned to structural oxygen in the bulk material, followed by hydroxide and carbonate peaks at ~530.4 and ~531.3 eV, respectively. The peaks at a higher binding energy are assigned to the species O−C═O (~532.3 eV) and C−O (~533.5 eV).[18] In Li 1s, the lowest binding energy peak at ~53.8 eV is assigned to structural Li in bulk NMC, followed by the peak with a higher binding energy within a range ~54.5 to ~54.9 eV assigned to $LiOH/Li_2CO_3$ in the surface.[15,16] The data did not allow for conclusive separation of these contributions, and therefore, these were fitted together as a slightly broader peak. The origin of the peak at around 56 eV binding energy in the Li 1s spectra is still unclear, and based on the vast variety of binding energy positions reported in literature,[17] a specific assignment is

https://doi.org/10.1021/acsaem.3c01621
ACS Appl. Energy Mater. 2023, 6, 11458−11467

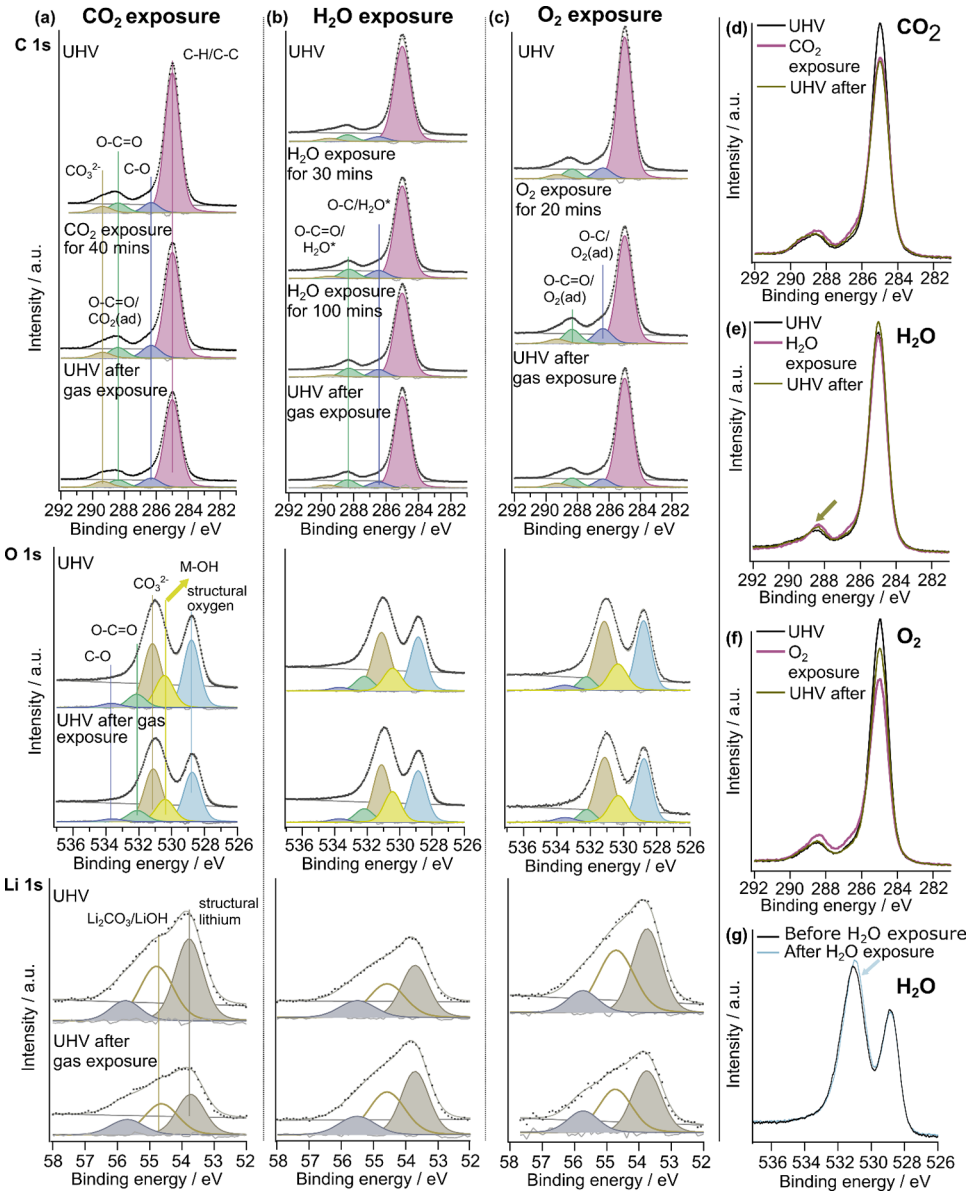

Figure 2. Curve-fitted C 1s ($h\nu$ = 435 eV), O 1s ($h\nu$ = 680 eV), and Li 1s ($h\nu$ = 435 eV) spectra measured under UHV before and after CO_2 (a), H_2O (b), and O_2 (c) gas exposure, C 1s ($h\nu$ = 435 eV) spectra were also obtained in ambient pressure during gas exposure; overlay plot of C 1s spectra obtained under UHV and CO_2 exposure (d), H_2O exposure (e), and O_2 exposure (f) and O 1s ($h\nu$ = 680 eV) carried out under UHV before and after H_2O exposure (g). The lines following the trend of the dots in (a), (b), and (c) are the sum of fitting.

omitted here. However, the binding energy and intensity of this feature remain constant throughout the experiment, and thus, the species giving this signal does not seem to participate in the surface composition changes. The above fitting information is listed in Table 2.

By comparing the C 1s, O 1s, and Li 1s spectra measured under UHV before and after CO_2 exposure, no obvious difference can be seen. Figure 2d shows the overlaid C 1 s spectra, while no change is seen between the UHV before and after exposure, and we can see a small increase in intensity of the O−C═O peak (~288.5 eV) in the C 1s spectrum when measured under gas pressure. This increase is suggested to originate from CO_2 gas adsorption on the sample surface.[23−28] In this case, CO_2 is likely chemisorbed to the surface since an increased intensity was observed at 288.5 eV binding energy. With a NiO [110] substrate, which is the most relevant material to NMC811 with similar Ni−O bonds, studies of gas adsorption show that the linear-physisorbed CO_2 gives a signal contribution of ~293 eV, whereas the bent-chemisorbed CO_2 feature contributes ~288 eV in the C 1s spectra.[29] In the obtained C 1s spectra, no peak can be observed at around 293 eV; see Figure S7 in Supporting Information. Thus, the contribution to peak at ~288.5 eV in this case is assigned to bent-chemisorbed CO_2 on the NMC 811 surface. In this work, the changes to the C 1s spectrum disappear under UHV conditions, which means that the weakly bound CO_2 can be desorbed from the NMC 811 surface. Scheme 1a illustrates a plausible bonding mechanism between the ideal, clean NMC surface and chemisorbed CO_2, where the oxygen atom from CO_2 gas bond to transition metals (mostly Ni). The chemisorbed CO_2 contains two oxygen atoms in different chemical environments, and as stated above, the one bonded to a metal gives a lower binding energy compared to an oxygen atom double bonded to a C atom. However, since no increased

https://doi.org/10.1021/acsaem.3c01621
ACS Appl. Energy Mater. 2023, 6, 11458−11467

Scheme 1. Proposed Reaction Mechanism of CO_2(a) and H_2O (b) Interaction with an Ideal, Clean NMC 811 Surface[a]

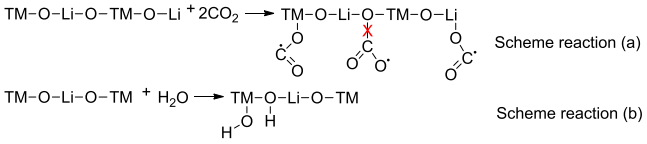

[a]The surface-adsorbed CO_2 is likely bonded to metal rather than surface oxygen. The surface-adsorbed H_2O Can transfer protons to nearby surface oxygen, leading to the formation of metal hydroxide. *TM refers to transition metals, i.e., Ni, Mn, and Co in this material.

intensity in carbonate species has been detected in the C 1s spectrum (Figure 2a), it is most likely that the bond between the surface oxygen from the NMC material and the CO_2 gas does not form. Upon UHV evacuation, these small intensity changes in the O=C–O species disappear, indicating that no permanent changes occurred to the surface composition of NMC 811 when exposed to pure CO_2. As observed in this experiment, CO_2 alone does not induce irreversible changes to the surface of NMC811 under low-pressure conditions (1.2×10^{-3} mbar) for a duration of 40 min.

H_2O Exposure. The sensitivity of NMC 811 toward H_2O was studied using the same methodology as described in CO_2 exposure section above. Figure 2b shows the curve-fitted C 1s, O 1s, and Li 1s spectra measured under UHV before and after water vapor exposure and, in addition, a C 1s spectrum measured during H_2O exposure (7×10^{-3} mbar) after 30 min exposure to H_2O. Unfortunately, the O 1s and Li 1s spectra under H_2O vapor pressure are omitted from analysis since these spectra could not be determined to be free from X-ray irradiation damage. The C 1s spectra measured under H_2O vapor show an increase in intensity around 286.5 and 288.5 eV binding energy compared to the spectrum measured under UHV before exposure. This enhancement in intensity suggests the adsorption of H_2O on the hydrocarbon and carbon oxide species residing on the NMC 811 surface and is indicated as H_2O* in the figures. From Figure 2e, it can be seen that the small increase in intensity remained once under UHV conditions. In Figure 2b, more observable changes were seen in the O 1s spectra obtained under UHV after gas exposure compared to those carried out before gas exposure. The peak assigned to metal hydroxide increased in intensity relative to the peak assigned to oxygen in the bulk structure after H_2O exposure. In the curve fit, the ratio of Area (–OH)/Area (structural oxygen) increased from 0.43 before H_2O exposure to 0.53 after H_2O exposure. The increase in hydroxide species on the surface is also clearly visible in the overlaid spectra in Figure 2g, and the broad peak at ~531 eV binding energy shifts toward the lower values in the O 1s spectrum obtained after H_2O exposure. It is suggested that H_2O initially chemisorbs on the NMC 811 surface, followed by a water splitting reaction where Ni–O–Li (mainly Ni–O bond) is working as the catalyst.[30−32] In the end, metal hydroxide species are produced, as presented in the suggested reaction scheme (Scheme 1b). Thus, in contrast to CO_2 exposure, a strong response is observed during short-term H_2O exposure (30 min) through formation of metal hydroxide on NMC 811.

O_2 Exposure. In order to determine if O_2 is involved in the surface degradation reaction, pristine NMC 811 was exposed to O_2 and monitored with APPES. As displayed in Figure 2c, the C 1s spectral features at 286.5 and 288.5 eV are enhanced under O_2 pressure (2.4×10^{-3} mbar) after exposure for ~20 min, which is assigned to O_2 surface adsorption.[33] It is most likely that the increased amount of carbon oxide species detected in the C 1s spectrum is caused by weak interactions between O_2 and pre-existing contaminations/carbon impurity species, i.e., C–H and C–O species but not NMC 811 itself, similar to the case of H_2O. The presence of carbon-based surface contaminants is expected for all NMC 811 materials from production and handling. In Figure 2c,f, no notable changes were found in C 1s, O 1s, and Li 1s under UHV measurements following O_2 exposure compared to the UHV measurements before O_2 exposure. This implies that the O_2 surface adsorption is reversible under UHV. We thus conclude that the O_2 exposure does not change the NMC 811 surface; however, it introduces carbon oxide species that reside in the NMC 811 surface during O_2 exposure.

Mixed Gas Conditions. In industry, Ni-rich NMC materials are commonly handled under dry room conditions as they maintain the battery performance. In the following measurements, the NMC 811 surface is exposed to two different gas mixtures, CO_2/O_2 and $CO_2/H_2O/O_2$, representing ambient atmospheres with different relative partial pressures of water (~10^{-6} and ~10^{-2} mbar), in order to identify the changes in the surface composition and relate this to a proposed reaction mechanism.

CO_2/O_2 Exposure. The exposure of NMC 811 to a mixture of CO_2 (5.6×10^{-4} mbar) and O_2 (3.3×10^{-2} mbar) gases leads to a similar result to when the material is exposed to the individual gases. Specifically, a clear growth can be seen in the O–C=O and C–O peak signals in C 1s and O 1s spectra in Figure 3a, partially assigned to the O_2 adsorption on the surface.[33] CO_2 chemisorption is also suggested to contribute to the increase in peak intensity observed in the O–C=O feature in the C 1s spectrum. At the same time, chemisorbed CO_2 also gives an intensity increase to the O 1s peak at ~531 and ~532 eV binding energy, thus overlapping with the contribution from O_2 adsorption. The structural oxygen peak shows relatively less intensity, indicating a thicker surface layer on top of the NMC 811 material compared to the one before gas exposure. The change in surface composition seen in the C 1s and O 1s spectra disappears when the sample is once again placed under UHV (see Figure 3a,c). This implies that the CO_2 and O_2 chemisorption products are not stable under UHV. The APPES data suggest that the CO_2 and O_2 gas mixture behaves like the sum of the two individual gases, with no extra correlated reactions.

$CO_2/H_2O/O_2$ Exposure. After determining the surface composition of NMC 811 under CO_2/O_2, it is motivated to introduce H_2O into the mixed gases in order to study the reversibility of the reactions on the NMC 811 surface with the presence of H_2O. In this case, the gas mixture consists of ~6.7×10^{-4} mbar CO_2, ~1.2×10^{-2} mbar O_2 and ~1.3×10^{-2} mbar H_2O summing to a total pressure of ~2.5×10^{-2} mbar. After gas exposure for ~55 min, as depicted in Figure 3b, the changes to the C 1s spectrum resembled that when NMC 811 is exposed to a mixture of CO_2 and O_2 gas. Chemical species O–C=O and C–O gain intensity in the C 1s spectrum, which is likewise assigned to the coadsorbed of CO_2 and O_2 gas on the NMC 811 surface.[25,29,33] From Figure 2f, it is expected that H_2O chemisorption will also contribute to the intensity of the C–O and O–C=O peaks.

https://doi.org/10.1021/acsaem.3c01621
ACS Appl. Energy Mater. 2023, 6, 11458−11467

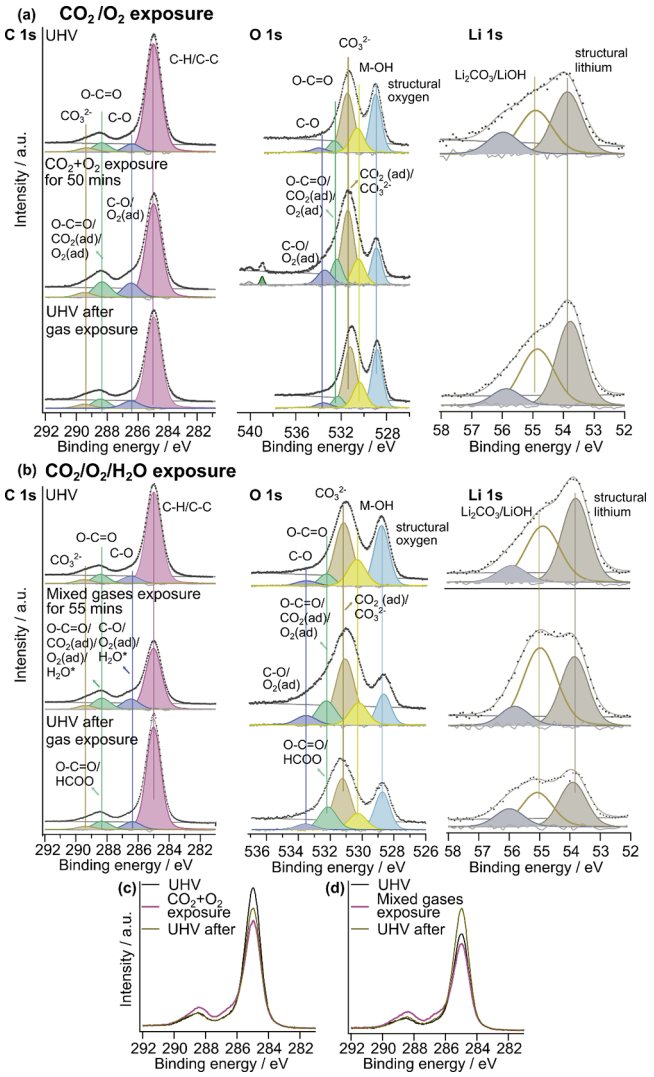

Figure 3. (a) C 1s (left, hν = 435 eV), O 1s (middle, hν = 680 eV), and Li 1s (right, hν = 435 eV) spectra carried out under UHV before gas exposure (top), in CO_2+O_2 mixed gases (middle in row), and under UHV after gas exposure (bottom); Li 1s is not included in any in situ measurements; (b) C 1s (left, hν = 435 eV), O 1s (middle, hν = 680 eV), and Li 1s (right, hν = 435 eV) spectra carried out under UHV before gas exposure (top), in CO_2+O_2+H_2O mixed gases (middle in row), and under UHV after gas exposure (bottom); (c) stack plot of C 1s measured under UHV and CO_2+O_2 gas pressures; (d) stack plot of C 1s measured under UHV and CO_2+O_2+H_2O gas pressures. The lines following the trend of the dots in (a) and (b) are the sum of fitting.

In O 1s in Figure 3b, the peaks assigned to O−C═O and C−O gain intensity under gas pressure, which is related to O_2 surface adsorption. In addition to that, chemisorbed CO_2 contributes to the intensity increase of peaks at ∼531 and ∼532 eV. Such surface adsorption is expected to occur in the presence of H_2O as it did for a mix of CO_2 and O_2 alone. Interestingly, when H_2O is present, the changes to C 1s and O 1s spectra do not completely disappear once placed back under UHV. This irreversible change implies that the presence of H_2O leads to more stable compounds and therefore irreversible surface changes. As displayed in Figure 3d, under UHV after mixed CO_2/H_2O/O_2 gas exposure, the C 1s peak assigned to O−C═O has a slightly higher intensity compared to the spectrum measured before gas exposure. The increased occupancy of hydrocarbon on the surface makes the changes in the O−C═O peak even less visible. In the spectrum of the O 1s obtained under UHV after gas exposure, the contribution of the CO_2 chemisorption was still detectable (see Figure 3b). With these results, it is most likely that the presence of H_2O stabilizes the chemisorbed CO_2 on the NMC 811 surface. A possible reaction mechanism is shown in Scheme 2, where

Scheme 2. Proposed Reaction Mechanism of CO_2 and H_2O Interaction with an Ideal, Clean NMC 811 Surface[a]

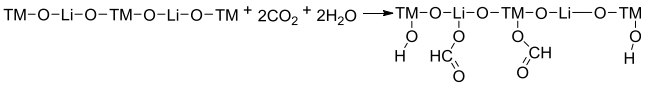

[a]Chemisorbed H_2O can transfer a proton to nearby chemisorbed CO_2, which is an oxygen atom bonding to a metal in the NMC 811 surface. *TM refers to transition metals, i.e., Ni, Mn, and Co in this material.

chemisorbed H_2O transfers a proton to nearby chemisorbed CO_2, thus forming a carboxylate on both lithium and TM sites. The carboxylate species is likely more stable than chemisorbed CO_2, thus inducing permanent changes to the NMC 811 surface.[25,34]

By comparing the Li 1s spectra obtained at near ambient pressure and under UHV conditions in Figure 3b, the intensity of the assigned Li_2CO_3/LiOH peak increases when measured under gas pressure, which might be due to the newly formed carboxylate and chemisorbed CO_2 on the lithium sites. While the UHV conditions are applied afterward, chemisorbed CO_2 on the Li atom is removed under UHV, correlating with the decreased intensity in the LiOH/Li_2CO_3 peak under UHV conditions.

Figure S2 in the Supporting Information shows the Ni 2p spectra measured under UHV before, during, and after this mixture gas exposure. No change in Ni 2p peak shape is observed, which may be expected as the chemical surrounding of the TM is still very similar for a nonideal NMC811 surface (surface termination groups are likely present).

In summary, exposure to O_2 and CO_2 leads only to surface-adsorbed gas molecules, which, in the time frame of these experiments, are readily removed under UHV conditions. However, the results show that the presence of H_2O alone first leads to the generation of surface hydroxides and second in the presence of CO_2 the generation of more stable carboxylate-like species. These two species are not removed under UHV and are proposed to be the first more permanent decomposition products formed when NMC 811 is exposed to air.

Effect of X-rays on Surface Composition with Ambient Pressure. The effect of X-rays on the surface composition is critical knowledge as the true surface degradation mechanism can only be determined once X-ray-induced effects are minimized or avoided. During the in situ measurements, it was observed that X-ray irradiation influenced the surface changes under both UHV and gas pressure conditions, with a higher extent under higher gas pressures. Below, the effects of X-ray irradiation are explained in detail.

X-ray Exposure under UHV Conditions. In order to understand and control the impact of radiation damage with X-ray exposure under ambient conditions, an initial starting point is to monitor X-ray-induced effects under UHV conditions. As we can see from Figure 4, after 1 or 2 min of

https://doi.org/10.1021/acsaem.3c01621
ACS Appl. Energy Mater. 2023, 6, 11458−11467

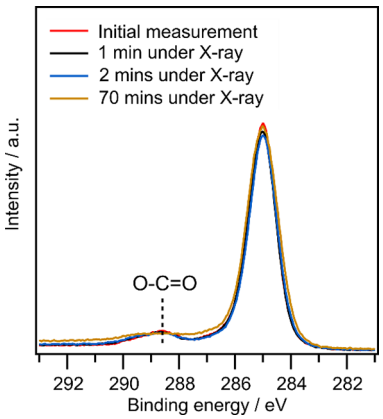

Figure 4. C 1s ($h\nu$ = 435 eV) spectra measured on NMC 811 after storage under UHV conditions with varying X-ray exposure time. The spectra were energy calibrated by referring to the highest peak point as 285 eV.

X-ray exposure, no noticeable changes can be observed in C 1s spectra compared to the initial spectrum that is obtained on a fresh spot. However, after 70 min exposure time, the peak intensity at ~288.5 eV substantially decreases, indicating that the O−C═O species decomposes when exposed to X-rays for an extended period of time.

Combined CO_2 and X-ray Exposure. In order to investigate the effect of X-ray irradiation on the formation of surface degradation products under ambient CO_2 pressure, during gas introduction, the C 1s and O 1s spectra were monitored as a function of gas pressure and X-ray exposure time. As can be seen in C 1s and O 1s heat maps (Figure 5a), the carbonate peak intensity at ~ 290 and 531.5 eV binding energy, respectively, grew substantially with a combined exposure of CO_2 gas and X-ray irradiation. At the start of the experiment, the CO_2 gas pressure increased from 1×10^{-6} to 1.2×10^{-3} mbar with10 min. Figure 5b shows integrated C 1s and O 1s spectra from the XPS heat maps and they represent four different gas exposure and beam irradiation times: before exposure to both CO_2 and X-rays (blue), after 6−8 min of exposure to both CO_2 and X-rays (green), after 20−22 min exposure to both CO_2 and X-rays (yellow), and finally after 25−27 min of exposure to only CO_2 on a fresh spot without X-ray exposure (red). The intensity of each spectrum is an average of 10 scans in the heat map between the lines of each associated color. After being exposed to X-rays and CO_2 for approximately 20 min, the carbonate peak in the C 1s and O 1s spectra (yellow spectra) shows higher intensity compared to the spectra measured on a spot that was not irradiated by X-rays and exposed to CO_2 for approximately 25 min (red spectra). This indicates that the formation of carbonate on the NMC 811 sample surface under CO_2 gas exposure is due to X-ray irradiation rather than the initial reaction between the CO_2 and NMC surface. Therefore, exposure to a high X-ray dose in a CO_2 atmosphere can lead to the generation of carbonate species rather than surface-adsorbed CO_2 in the absence of any other factors (e.g., the presence of H_2O). Comparing the C 1s spectrum measured under UHV before CO_2 exposure (blue) to the spectrum obtained under CO_2 pressure (red), we can see a small increase in intensity of the carbonate peak in the spectra (red). This difference is attributed to X-ray irradiation as no formation of carbonates was seen when the surface was exposed to only CO_2 gas (see Figure 2a). The red spectrum was measured for approximately 2 min, and this demonstrates

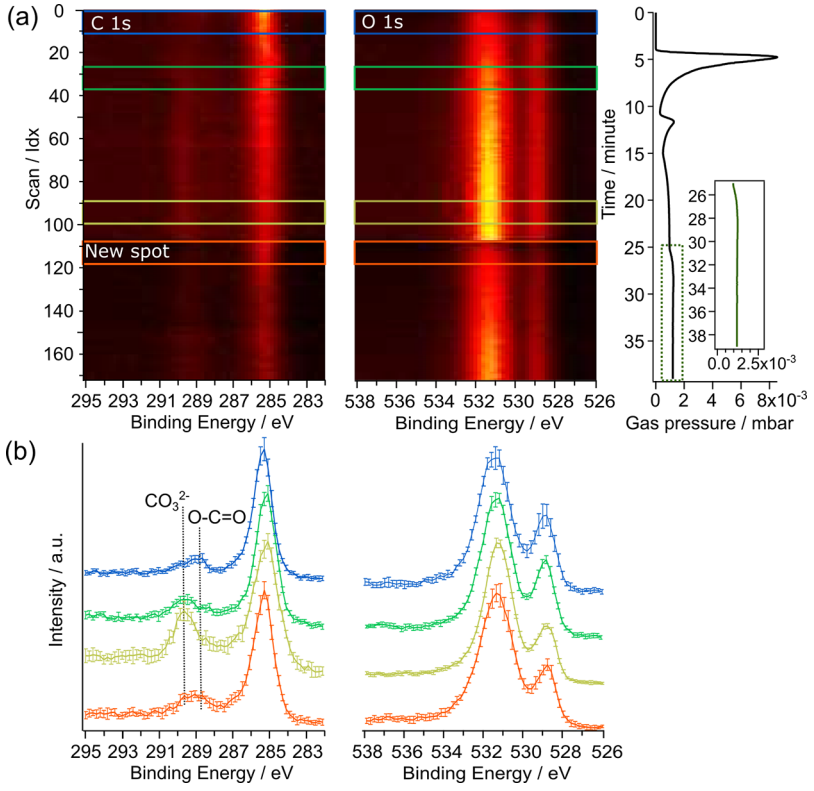

Figure 5. Heat maps (a) and spectra (b) of C 1s ($h\nu$ = 680 eV) and O 1s ($h\nu$ = 680 eV) during CO_2 introduction as a function of beam irradiation time and CO_2 gas pressure (right).

https://doi.org/10.1021/acsaem.3c01621
ACS Appl. Energy Mater. 2023, 6, 11458−11467

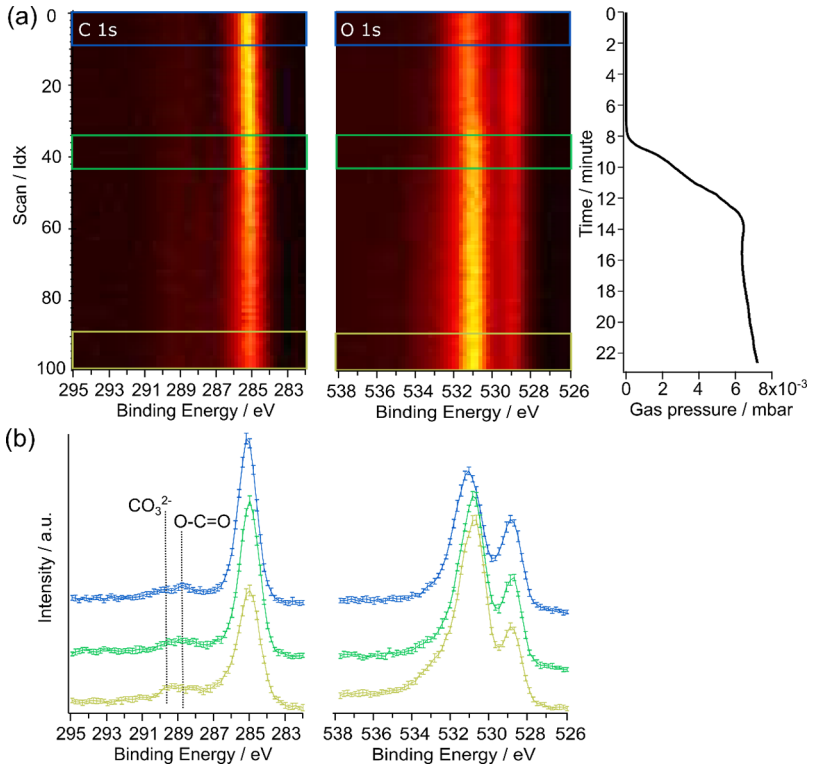

Figure 6. Heat maps (a) and spectra (b) of C 1s ($h\nu$ = 680 eV) and O 1s ($h\nu$ = 680 eV) during H_2O introduction as a function of beam irradiation time and gas pressure (right).

that the X-ray damage is enhanced by the presence of CO_2 gas. As a final note, X-ray irradiation plays a crucial role in the formation of carbonate on the NMC 811 surface under CO_2 gas pressure, and if not minimizing the influence of X-rays, a completely different conclusions would be drawn.

Combined H_2O and X-ray Exposure. Similarly, the effects of the X-ray irradiation time in ambient H_2O on NMC 811 were investigated. In the C 1s heat map, a lower intensity can be detected from C−H species after ∼15 min of exposure to both H_2O and X-rays (see Figure 6a). From the heat maps of the O 1s and gas pressure during the measurements, it can be seen that the peak at ∼531 eV increased in intensity when H_2O is present. To compare the change in the C 1s and O 1s spectra, integration of 10 scans at various stages of the experiment is shown in Figure 6b. The integrated C 1s and O 1s spectra collected before exposure to both H_2O and X-rays are shown in blue, those collected after 0−2 min of exposure to both H_2O and X-rays are shown in green, and those collected after 15−17 min exposure to both H_2O and X-rays are shown in yellow. In the O 1s spectra, a peak at ∼531 eV shifts toward lower value as the exposure time increases, which is consistent with that expected from the formation of metal hydroxide described above (Figure 2b). No major influence can thus be observed for the formation of metal hydroxide due to X-rays. On the contrary, in Figure 6b, the carbonate peak (∼290 eV binding energy) in the C 1s spectrum (red) obtained after X-ray irradiation for ∼15−17 min has a higher intensity relative to the spectrum (blue) collected before exposure to both X-rays and H_2O, indicating that a small amount of carbonates formed due to the combined H_2O and X-ray exposure. Reaction between H_2O and O−C═O on the NMC 811 surface might produce carbonate under X-ray irradiation after ∼15 min.

CONCLUSIONS

In this work, it was demonstrated that by placing NMC 811 under UHV conditions, the carbonate impurity species formed during material synthesis and storage are to a large extent removed. This may possibly be utilized in both industry and research fields for electrode preparation as batteries based on NMC 811 electrodes with fewer carbonates on the surface are known to have a lower overpotential. During in situ measurements, it shows that after exposure to singular CO_2, or O_2 gas and a mixture of CO_2/O_2 gases, the chemical composition on the NMC 811 surface does not undergo permanent modification. However, irreversible reactions were observed when H_2O vapor was incorporated either separately or in a $CO_2/H_2O/O_2$ mixture. That is, even following the application of UHV, formation of metal hydroxide and carboxylate remains after H_2O and the mixed $CO_2/H_2O/O_2$ gas exposure, respectively. It is suggested that the presence of H_2O can stabilize surface adsorbed CO_2 by transferring a proton and forming carboxylate which is not observed under coadsorption of CO_2 and O_2. We thus conclude that the presence of H_2O is necessary for triggering the formation of detrimental surface deposits. Unlike many other studies claiming that carbonate is the main degrading species on the NMC 811 surface under storage, this work presents the initial reaction between NMC 811 and H_2O/CO_2 in a short-time period (within 1 h) and demonstrates that carboxylate is the initial product in the degradation process. Finally, it is demonstrated that extended exposure to a combination of gas (CO_2 or H_2O) and X-rays exhibits generation of carbonates on the surface of NMC 811. Thus, this result provides a cautionary tale to battery scientists when studying material degradation via advanced X-ray methods and provides insight into how to avoid misleading results.

https://doi.org/10.1021/acsaem.3c01621
ACS Appl. Energy Mater. 2023, 6, 11458−11467

■ ASSOCIATED CONTENT

Supporting Information

The Supporting Information is available free of charge at https://pubs.acs.org/doi/10.1021/acsaem.3c01621.

SEM image and XRD pattern of NMC 811 materials; Ni 2p spectra; Co 2p and Mn 2p spectra; survey spectrum; C 1s spectra collected under various temperatures; C 1s spectra measured on three fresh spots; and C 1s spectra obtained before and after CO2 exposure (PDF)

■ AUTHOR INFORMATION

Corresponding Authors

Heyin Chen − *Department of Chemistry − Ångström Laboratory, Uppsala University, 751 20 Uppsala, Sweden;* orcid.org/0000-0001-6684-6373; Email: heyin.chen@kemi.uu.se

Maria Hahlin − *Department of Chemistry − Ångström Laboratory, Uppsala University, 751 20 Uppsala, Sweden; Department of Physics and Astronomy, Uppsala University, 75120 Uppsala, Sweden;* orcid.org/0000-0002-5680-1216; Email: maria.hahlin@kemi.uu.se

Authors

Tove Ericson − *Department of Chemistry − Ångström Laboratory, Uppsala University, 751 20 Uppsala, Sweden*

Robert H. Temperton − *MAX IV Laboratory, Lund University, 221 00 Lund, Sweden;* orcid.org/0000-0002-4802-6862

Ida Källquist − *Department of Physics and Astronomy, Uppsala University, 75120 Uppsala, Sweden*

Haidong Liu − *Department of Chemistry − Ångström Laboratory, Uppsala University, 751 20 Uppsala, Sweden;* orcid.org/0000-0001-8519-3240

Calley N. Eads − *MAX IV Laboratory, Lund University, 221 00 Lund, Sweden*

Anastasiia Mikheenkova − *Department of Chemistry − Ångström Laboratory, Uppsala University, 751 20 Uppsala, Sweden*

Margit Andersson − *MAX IV Laboratory, Lund University, 221 00 Lund, Sweden*

Esko Kokkonen − *MAX IV Laboratory, Lund University, 221 00 Lund, Sweden;* orcid.org/0000-0002-3674-7486

William R. Brant − *Department of Chemistry − Ångström Laboratory, Uppsala University, 751 20 Uppsala, Sweden*

Complete contact information is available at: https://pubs.acs.org/10.1021/acsaem.3c01621

Notes

The authors declare no competing financial interest.

■ ACKNOWLEDGMENTS

We gratefully acknowledge the Swedish Energy Agency (48678-1, 40495-1), Swedish Research Council (2020-04512, 2018-06465), and STandUP for energy for financial support. We also acknowledge MAX IV Laboratory for time on SPECIES Beamline (proposal #20200670 and #20211068). Research conducted at the MAX IV Laboratory, a Swedish national user facility, is supported by the Swedish Research council under contract 2018-07152, the Swedish Governmental Agency for Innovation Systems under contract 2018-04969, and Formas under contract 2019-02496. The authors would like to thank Yonas Tesfamhret and Andrew J. Naylor (Uppsala University) for the helpful input.

■ REFERENCES

(1) Castelvecchi, D. Electric cars and batteries: how will the world produce enough? *Nature* **2021**, *596*, 336−339.

(2) Noh, H.-J.; Youn, S.; Yoon, C. S.; Sun, Y.-K. Comparison of the structural and electrochemical properties of layered $Li[Ni_xCo_yMn_z]O_2$ (x = 1/3, 0.5, 0.6, 0.7, 0.8 and 0.85) cathode material for lithium-ion batteries. *J. Power Sources* **2013**, *233*, 121−130.

(3) Julien, C. M.; Mauger, A. NCA, NCM811, and the Route to Ni-Richer Lithium-Ion Batteries. *Energies* **2020**, *13* (23), 6363.

(4) Zhang, L.; Müller Gubler, E. A.; Tai, C.-W.; Kondracki, Ł.; Sommer, H.; Novák, P.; El Kazzi, M.; Trabesinger, S. Elucidating the Humidity-Induced Degradation of Ni-Rich Layered Cathodes for Li-Ion Batteries. *ACS Appl. Mater. Interfaces* **2022**, *14* (11), 13240−13249.

(5) Jung, R.; Metzger, M.; Maglia, F.; Stinner, C.; Gasteiger, H. A. Oxygen Release and Its Effect on the Cycling Stability of $LiNi_xMn_yCo_zO_2$(NMC) Cathode Materials for Li-Ion Batteries. *J. Electrochem. Soc.* **2017**, *164* (7), A1361−A1377.

(6) Dose, W. M.; Temprano, I.; Allen, J. P.; Björklund, E.; O'Keefe, C. A.; Li, W.; Mehdi, B. L.; Weatherup, R. S.; De Volder, M. F. L.; Grey, C. P. Electrolyte Reactivity at the Charged Ni-Rich Cathode Interface and Degradation in Li-Ion Batteries. *ACS Appl. Mater. Interfaces* **2022**, *14* (11), 13206−13222.

(7) Jung, R.; Morasch, R.; Karayaylali, P.; Phillips, K.; Maglia, F.; Stinner, C.; Shao-Horn, Y.; Gasteiger, H. A. Effect of Ambient Storage on the Degradation of Ni-Rich Positive Electrode Materials (NMC811) for Li-Ion Batteries. *J. Electrochem. Soc.* **2018**, *165* (2), A132−A141.

(8) Andersen, H. L.; Cheung, E. A.; Avdeev, M.; Maynard-Casely, H. E.; Abraham, D. P.; Sharma, N. Consequences of long-term water exposure for bulk crystal structure and surface composition/chemistry of nickel-rich layered oxide materials for Li-ion batteries. *J. Power Sources* **2020**, *470*, No. 228370.

(9) Faenza, N. V.; Bruce, L.; Lebens-Higgins, Z. W.; Plitz, I.; Pereira, N.; Piper, L. F. J.; Amatucci, G. G. Editors' Choice—Growth of Ambient Induced Surface Impurity Species on Layered Positive Electrode Materials and Impact on Electrochemical Performance. *J. Electrochem. Soc.* **2017**, *164* (14), A3727−A3741.

(10) Sicklinger, J.; Metzger, M.; Beyer, H.; Pritzl, D.; Gasteiger, H. A. Ambient Storage Derived Surface Contamination of NCM811 and NCM111: Performance Implications and Mitigation Strategies. *J. Electrochem. Soc.* **2019**, *166* (12), A2322−A2335.

(11) He, Y.; Liu, Z.; Jia, H.; Zhu, J.; Zheng, J.; Wang, G.; Li, X.; Xiao, J.; Liu, J.; Zhang, J. G.; Chen, G.; Wang, C. Unlocking the passivation nature of the cathode-air interfacial reactions in lithium ion batteries. *Nat. Commun.* **2020**, *11* (1), 3204.

(12) Motzko, M.; Carrillo Solano, M. A.; Jaegermann, W.; Hausbrand, R. Photoemission Study on the Interaction Between $LiCoO_2$ Thin Films and Adsorbed Water. *J. Phys. Chem. C* **2015**, *119* (41), 23407−23412.

(13) Gao, Y.; Jiang, R.; Dai, Z.; Du, Z.; Jin, Y.; Li, G.; Hou, S. Revealing the Relationships between Washing/Recalcination Processes and Structure Performance of Ni-Rich Layered Cathode Materials. *ACS Appl. Energy Mater.* **2022**, *5* (12), 15059−15077.

(14) Kokkonen, E.; Lopes da Silva, F.; Mikkela, M. H.; Johansson, N.; Huang, S. W.; Lee, J. M.; Andersson, M.; Bartalesi, A.; Reinecke, B. N.; Handrup, K.; Tarawneh, H.; Sankari, R.; Knudsen, J.; Schnadt, J.; Sathe, C.; Urpelainen, S. Upgrade of the SPECIES beamline at the MAX IV Laboratory. *J. Synchrotron Radiat.* **2021**, *28* (Pt 2), 588−601.

(15) Kozen, A. C.; Pearse, A. J.; Lin, C.-F.; Schroeder, M. A.; Noked, M.; Lee, S. B.; Rubloff, G. W. Atomic Layer Deposition and in Situ Characterization of Ultraclean Lithium Oxide and Lithium Hydroxide. *J. Phys. Chem. C* **2014**, *118* (48), 27749−27753.

(16) Yao, K. P. C.; Kwabi, D. G.; Quinlan, R. A.; Mansour, A. N.; Grimaud, A.; Lee, Y.-L.; Lu, Y.-C.; Shao-Horn, Y. Thermal Stability of

$Li_2O_2$and Li_2O for Li-Air Batteries: In Situ XRD and XPS Studies. *J. Electrochem. Soc.* **2013**, *160* (6), A824−A831.
(17) Wood, K. N.; Teeter, G. XPS on Li-Battery-Related Compounds: Analysis of Inorganic SEI Phases and a Methodology for Charge Correction. *ACS Appl. Energy Mater.* **2018**, *1* (9), 4493−4504.
(18) Bichon, M.; Sotta, D.; Dupré, N.; De Vito, E.; Boulineau, A.; Porcher, W.; Lestriez, B. Study of Immersion of $LiNi_{0.5}Mn_{0.3}Co_{0.2}O_2$ Material in Water for Aqueous Processing of Positive Electrode for Li-Ion Batteries. *ACS Appl. Mater. Interfaces* **2019**, *11* (20), 18331−18341.
(19) Liu, H.; Naylor, A. J.; Menon, A. S.; Brant, W. R.; Edström, K.; Younesi, R. Understanding the Roles of Tris(trimethylsilyl) Phosphite (TMSPi) in $LiNi_{0.8}Mn_{0.1}Co_{0.1}O_2$(NMC811)/Silicon−Graphite (Si−Gr) Lithium-Ion Batteries. *Adv. Mater. Interfaces* **2020**, *7* (15), No. 2000277.
(20) Azmi, R.; Masoumi, M.; Ehrenberg, H.; Trouillet, V.; Bruns, M. Surface analytical characterization of $LiNi_{0.8}$-yMn yCo $_{0.2}O_2$($0 \leq y \leq 0.4$) compounds for lithium-ion battery electrodes. *Surf. Interface Anal.* **2018**, *50* (11), 1132−1137.
(21) Hekmatfar, M.; Kazzazi, A.; Eshetu, G. G.; Hasa, I.; Passerini, S. Understanding the Electrode/Electrolyte Interface Layer on the Li-Rich Nickel Manganese Cobalt Layered Oxide Cathode by XPS. *ACS Appl. Mater. Interfaces* **2019**, *11* (46), 43166−43179.
(22) Wood, M.; Li, J.; Ruther, R. E.; Du, Z.; Self, E. C.; Meyer, H. M.; Daniel, C.; Belharouak, I.; Wood, D. L. Chemical stability and long-term cell performance of low-cobalt, Ni-Rich cathodes prepared by aqueous processing for high-energy Li-Ion batteries. *Energy Storage Mater.* **2020**, *24*, 188−197.
(23) Kim, J.; Ha, H.; Doh, W. H.; Ueda, K.; Mase, K.; Kondoh, H.; Mun, B. S.; Kim, H. Y.; Park, J. Y. How Rh surface breaks CO_2 molecules under ambient pressure. *Nat. Commun.* **2020**, *11* (1), 5649.
(24) Eren, B.; Heine, C.; Bluhm, H.; Somorjai, G. A.; Salmeron, M. Catalyst Chemical State during CO Oxidation Reaction on Cu(111) Studied with Ambient-Pressure X-ray Photoelectron Spectroscopy and Near Edge X-ray Adsorption Fine Structure Spectroscopy. *J. Am. Chem. Soc.* **2015**, *137* (34), 11186−11190.
(25) Acta Chemica Scandinavica, S. A. P. A. I. C.; Hao; Rameshan, C.; Bukhtiyarov, A. V.; Prosvirin, I. P.; Bukhtiyarov, V. I.; Rupprechter, G. CO_2 activation on ultrathin ZrO_2 film by H_2O co-adsorption: In situ NAP-XPS and IRAS studies. *Surf. Sci.* **2019**, *679*, 139−146.
(26) Yang, C.; Bebensee, F.; Chen, J.; Yu, X.; Nefedov, A.; Woll, C. Carbon Dioxide Adsorption on CeO(2) (110): An XPS and NEXAFS Study. *ChemPhysChem* **2017**, *18* (14), 1874−1880.
(27) Yang, T.; Gu, T.; Han, Y.; Wang, W.; Yu, Y.; Zang, Y.; Zhang, H.; Mao, B.; Li, Y.; Yang, B.; Liu, Z. Surface Orientation and Pressure Dependence of CO_2 Activation on Cu Surfaces. *J. Phys. Chem. C* **2020**, *124* (50), 27511−27518.
(28) Ding, X.; De Rogatis, L.; Vesselli, E.; Baraldi, A.; Comelli, G.; Rosei, R.; Savio, L.; Vattuone, L.; Rocca, M.; Fornasiero, P.; Ancilotto, F.; Baldereschi, A.; Peressi, M. Interaction of carbon dioxide with Ni(110): A combined experimental and theoretical study. *Phys. Rev. B* **2007**, *76* (19), No. 195425.
(29) Illing, G.; Heskett, D.; Plummer, E.; Freund, H.; Somers, J.; Lindner, T.; Bradshaw, A.; Buskotte, U.; Neumann, M.; Starke, U. Adsorption and reaction of CO_2 on Ni {110}: X-ray photoemission, near-edge X-ray absorption fine-structure and diffuse leed studies. *Surf. Sci.* **1988**, *206* (1−2), 1−19.
(30) Kato, H.; Asakura, K.; Kudo, A. Highly Efficient Water Splitting into H_2 and O_2 over Lanthanum-Doped $NaTaO_3$ Photocatalysts with High Crystallinity and Surface Nanostructure. *J. Am. Chem. Soc.* **2003**, *125* (10), 3082−3089.
(31) Qiu, Z.; Ma, Y.; Edvinsson, T. In operando Raman investigation of Fe doping influence on catalytic NiO intermediates for enhanced overall water splitting. *Nano Energy* **2019**, *66*, No. 104118.
(32) QayoomMugheri, A.; Tahira, Aneela; Aftab, U.; Ishaq Abro, M.; Chaudhry, S. R.; Amaral, L.; Ibupoto, Z. H. Co_3O_4/NiO bifunctional electrocatalyst for water splitting. *Electrochim. Acta* **2019**, *306*, 9−17.
(33) Lee, W. H.; Lee, J. G.; Reucroft, P. J. XPS study of carbon fiber surfaces treated by thermal oxidation in a gas mixture of $O_2/(O_2+N_2)$. *Appl. Surf. Sci.* **2001**, *171* (1), 136−142.
(34) Vesselli, E.; Rizzi, M.; De Rogatis, L.; Ding, X.; Baraldi, A.; Comelli, G.; Savio, L.; Vattuone, L.; Rocca, M.; Fornasiero, P.; Baldereschi, A.; Peressi, M. Hydrogen-Assisted Transformation of CO_2 on Nickel: The Role of Formate and Carbon Monoxide. *J. Phys. Chem. Lett.* **2010**, *1* (1), 402−406.

https://doi.org/10.1021/acsaem.3c01621
ACS Appl. Energy Mater. 2023, 6, 11458−11467